QUARTERLY JOURNAL OF THE ROYAL METEOROLOGICAL SOCIETY
Q. J. R. Meteorol. Soc. **133**: (S2) 151–162 (2007)
Published online in Wiley InterScience
(www.interscience.wiley.com) DOI: 10.1002/qj.151

RMetS
ROYAL METEOROLOGICAL SOCIETY

Prediction of cloud ice signatures in submillimetre emission spectra by means of ground-based radar and *in situ* microphysical data

B. Rydberg,[a]* P. Eriksson[a] and S. A. Buehler[b]
[a] *Dept. of Radio and Space Science, Chalmers University of Technology, Gothenburg, Sweden*
[b] *Dept. of Space Science, Luleå Technical University, Kiruna, Sweden*

ABSTRACT: Submillimetre down-looking radiometry is a promising technique for global measurements of cloud ice properties. There exist no observation data of sufficient size that can be used for detailed pre-launch studies of such an instrument and other means must be found to obtain data to optimise the instrument design and similar tasks. Several aspects of the observations make traditional retrieval methods not suitable and nonlinear multidimensional regression techniques (e.g. Bayesian Monte Carlo integration and neural networks) must be applied. Such methods are based on a retrieval database and to be successful the database must mimic relevant real conditions closely. A method to generate such databases of high quality is described here. Correct vertical distributions of cloud ice are obtained by basic data from ground-based radars. Cloud ice particle microphysical properties are generated randomly where statistical parameters are selected to mimic *in situ* measurement data closely. Atmospheric background fields from ECMWF are perturbed to account for variation on sub-grid scales. All these data, together with sensor characteristics, are fed into a state-of-the-art radiative transfer simulator (ARTS). The method was validated by a successful comparison with AMSU data. Copyright © 2007 Royal Meteorological Society

KEY WORDS retrieval database; microwave remote sounding; microphysics

Received 14 February 2007; Revised 5 June 2007; Accepted 27 July 2007

1. Introduction

Ice clouds play an important role in Earth's radiation balance and climate because they reflect sunlight and trap infrared radiation. The net effect depends mainly on the clouds' optical depth and height. Poor knowledge of cloud processes is a main uncertainty for the prediction of the future climate (IPCC, 2001). From existing climate models, it is not even known whether cirrus clouds as a class would have a negative or positive feedback in climate change (Cess, 1996; IPCC, 2001).

The global knowledge of the physically most basic cloud parameters, the vertically integrated cloud ice mass (ice water path, IWP), and the particle size distribution (PSD) is poor and limited. The PSD determines the cloud radiative effect per mass and the cloud lifetime through ice particle fall speed. These ice cloud variables are difficult to retrieve from existing remote observations. This is mainly because a remote-sounding instrument is most sensitive to ice particles having a similar size to the wavelength used. Cloud ice particles have sizes in the range from μm to cm, and no general parametrization of microphysical properties (e.g. PSD and particle shapes) can be applied to all clouds, since these quantities are highly variable (Heymsfield and McFarquhar, 2002). Visible, infrared, and millimetre-wave measurements operate accordingly at the ends of the PSD, and in order to deduce an ice mass from such measurements, assumptions of the complete PSD are required. Furthermore, visible and near-infrared methods work only during daytime, and are most sensitive to the particles at the cloud top. Thermal infrared methods saturate for clouds with moderate optical depth, and millimetre-wave methods have low sensitivity for optically thinner clouds. The consequence is that mean values of IWP in global climate models can differ by an order of magnitude (Del Genio, 2002; John and Soden, 2006). Accordingly there exists a strong need for more accurate global observations of ice cloud masses.

Measurement of the cloud ice mass by down-looking submillimetre radiometry has been suggested (Evans *et al*., 2002; Buehler, 2005). The advantage of observing ice clouds in the submillimetre region is that the wavelengths are comparable with particle sizes representing most of the ice mass, and the induced brightness temperature change is largely proportional to the ice mass (Evans and Stephens, 1995; Gasiewski, 1992). Satellite submillimetre sensors do exist, but are all of the limb-sounding type. These instruments have confirmed the potential of submillimetre radiometry (Li *et al*., 2005; Eriksson *et al*.,

* Correspondence to: B. Rydberg, Department of Radio and Space Science, Chalmers University of Technology, SE-412 96 Gothenburg, Sweden. E-mail: benryd@chalmers.se

2007), but the measurements are limited to the orbit plane and the observation geometry results in poor horizontal resolution and altitude coverage.

Geophysical quantities are often retrieved from passive atmospheric sounding data in a Bayesian manner, where statistical *a priori* information is used to stabilize the often ill-posed problem. The most likely Bayesian solution can be found by analytical expressions if the involved quantities follow Gaussian statistics (Rodgers, 2000), but this is not a practical approach for cloud ice properties. As a solution to this, a Bayesian regression method has been presented by Evans *et al*. (2002). Another option to find the Bayesian solution is to apply neural networks, as done by Jiménez *et al*. (2003).

Both these retrieval approaches require an *a priori* retrieval database consisting of realistic atmospheric states and corresponding radiative transfer simulations, including the characteristics of the sensor. The retrieval database must mimic reality as closely as possible, by covering all possible states and exhibiting correct statistical properties. Evans *et al*. (2002) created retrieval database cloud profiles in a stochastic way. The cloud-top and cloud-base heights are picked from a probability density function (PDF) obtained from radar measurements. At these two heights, median mass particle diameter and ice water content values are selected from a PDF obtained from *in situ* measurements. The modelled ice cloud is then specified by these numbers.

The aim here is to further elaborate the creation of the database. This work is also based on ground-based cloud radars, but here the full information content of the radar observations is preserved. This is achieved by ensuring that ice water content and assumed microphysical properties are consistent with the basic radar observation, but not by relying on externally retrieved cloud ice profiles or derived data products. Furthermore, microphysical variables are randomly selected to reproduce the variation seen in data obtained from *in situ* measurement campaigns. Temperature and humidity fields from the European Centre for Medium-range Weather Forecasts (ECMWF) are perturbed to account for unresolved variability. The alternative option to use data from aircraft measurement campaigns with millimetre and submillimetre sensors on board (Evans *et al*., 2005) was considered not to be feasible. Existing datasets lack both required size and generality to be of interest for the purpose of building up a retrieval database. In addition, underlying microphysical properties are still unknown, with the consequence that a number of assumptions must still be made.

We focus our efforts here on the question of blending information from radars and *in situ* observations, and make a restriction to generate only 1D atmospheric states (i.e. all quantities depending only on altitude). Methods to convert time series of ground-based radar observations to 3D structured cloud fields have been presented (Hogan and Kew, 2005; Evans and Wiscombe, 2004). Correct 3D cloud fields are required to investigate some retrieval aspects, such as to quantify the additional retrieval error caused by applying an 'independent pixel approach' (Davis *et al*., 2006), where 1D conditions are assumed locally for each retrieval.

The scope of the paper is mainly to present an algorithm for generating ice cloud retrieval databases. The radar data used are from a rather narrow geographical area. The algorithm is general, and can easily take CloudSAT radar data as input. This will enable the creation of global retrieval databases.

2. Observations and data

2.1. Radar data and weather information

Ground-based cloud radars (35 and 94 GHz) were selected as the main information source for the spatial distribution of clouds. The main reasons for this choice are that the radars are operated continuously, provide large datasets and handle both thick and multi-layer clouds. In principle ground-based lidar data could be considered, but those instruments have a sensitivity to clouds which is quite different from down-looking submillimetre observations. This is because many ice cloud systems are impenetrable from below by the lidar signal, and hence thicker clouds (which submillimetre-wave observations are suitable for detecting) would not be well represented in the generated dataset.

The most basic radar observation parameter is the backscatter cross-section, normally reported as radar reflectivity, Z. Equivalent radar reflectivity is defined as

$$Z_{\mathrm{e}} = \frac{\lambda_{\mathrm{r}}^4}{4\pi^4 |K_{\mathrm{w}}(\lambda_{\mathrm{r}})|^2} \int_0^\infty \xi_{\mathrm{b}}(D, \lambda_{\mathrm{r}}) D^2 n(D)\, \mathrm{d}D, \qquad (1)$$

where Z_{e} is used instead of Z to indicate the possibility of non-Rayleigh scattering, λ_{r} is the wavelength of the radar, K_{w} is the dielectric factor of liquid water, ξ_{b} is the backscatter efficiency, D is the particle dimension, and $n(D)$ is the PSD. Data from the following midlatitude radar stations are considered:

1. Chilbolton, UK, 51.144 °N, 1.437 °W, 94 GHz, operated by RCRU, Rutherford Appleton Laboratory.
2. SIRTA, Palaiseau, Paris, France, 48.713 °N, 2.204 °E, 94 GHz, operated by CNRS/IPSL.
3. Cabauw, The Netherlands, 51.971 °N, 4.927 °E, 35 GHz, operated by the Netherlands weather sevice (KNMI).

The vertical resolution of the radars is better than 100 m. The data were obtained through the archive hosted by the CloudNET program (www.cloud-net.org, where more technical information can be found). Liquid water content profiles (level 2 meteorological products) are also taken from this archive.

Temperature, humidity and wind speed information for the time and location of the radar measurements are taken from the ECMWF weather model.

DOI: 10.1002/qj

2.2. Microphysical data

Assumptions on ice cloud microphysical parameters are mainly based on results from the *in situ* measurements reported by Ivanova *et al.* (2001), Heymsfield (2003b), and Korolev and Isaac (2003). Ivanova *et al.* (2001) investigated PSDs in non-convective midlatitude cirrus, using measurements by a Forward Scattering Spectrometer Probe and a laser imaging two-dimensional cloud (2DC) probe, from flights during the Atmospheric Radiation Measurement (ARM) and First ISCCP Radiation Experiment (FIRE) campaigns. Heymsfield (2003b) obtained data on PSDs from aircraft Lagrangian spirals and balloon-borne ascents through ice cloud layers of synoptically generated clouds. Particle sizes were measured by Particle Measurement System 2DC and two-dimensional precipitation (2DP) probes. Data were collected during the FIRE I campaign in the autumn of 1986 in Wisconsin, the FIRE II campaign in November and December 1991 in Kansas, and the ARM campaign in March 2000 in Oklahoma. Korolev and Isaac (2003) analysed particle shapes, measured by a cloud particle imager (CPI) probe. Data used were collected in winter midlatitude and polar clouds, during December 1997 to February 1998 in the Great Lakes Region, the Canadian and US Arctic in April 1998, and over Southern Ontario and Montreal region between November 1999 and February 2000.

3. Construction of the database

The database of concern consists of atmospheric states and corresponding simulated instrument measurements. The database must mimic reality as closely as possible, and must therefore cover all possible states and exhibit correct statistical properties. A main consideration is that no spurious correlation between data elements is introduced. The most important part of the procedure is to fill the database with atmospheric states, where the ice water content (IWC) profiles are distributed according to reality, and the underlying microphysical properties of the clouds and atmospheric background states are spread over their range of variability. The overall flow scheme of the database generation is:

1. Time series of radar backscatter cross-sections are averaged.
2. Vertical profiles of temperature, humidity and liquid water content are created.
3. Vertical profiles of ice cloud microphysical parameters are computed.
4. IWC profiles are computed (consistent with 1 to 3).
5. Radiative transfer calculations are performed.

Each step is described in more detail below.

3.1. Radar profile averaging

A radar measurement has a very fine horizontal resolution compared to the typical footprint size (several kilometres) for a satellite radiometric measurement. A single radar backscatter profile is thus not representative for footprint-averaged conditions, as clouds are normally highly structured in all spatial dimensions.

A simple way to partly overcome the difference in horizontal resolution is to use averaged radar data, instead of single observations. Direct time averages will correspond to different horizontal distances, so a better approach is to use the wind speed to create an average that matches the footprint size. Mean radar reflectivities are then calculated as

$$\overline{Z_{\mathrm{e}}} = \frac{\int_0^{t_0} Z_{\mathrm{e}}(t) v(t)\,\mathrm{d}t}{\int_0^{t_0} v(t)\,\mathrm{d}t},$$
$$\int_0^{t_0} v(t)\,\mathrm{d}t = x, \tag{2}$$

where $v(t)$ is the wind speed and x is the footprint size.

3.2. Temperature, humidity and liquid water content

Temperature and humidity profiles are taken from the ECMWF weather model, for the time and location of the radar measurements. These profiles are slightly modified by adding finer structures; this is to account for local variability not resolved by the ECMWF model. The additional term is generated in a random manner.

Several methods exist for creating random data with prescribed statistical characteristics. A method based on Cholesky decompositions is applied here. Random vectors, $\mathbf{x}$, with mean state $\overline{\mathbf{x}}$ and covariance matrix $\mathbf{S_x}$, can be generated as

$$\mathbf{x} = \overline{\mathbf{x}} + \mathbf{K}\mathbf{v}, \tag{3}$$

where $\mathbf{K}$ is the Cholesky decomposition of $\mathbf{S_x}$, a lower triangular matrix fulfilling $\mathbf{K}\mathbf{K}^{\mathrm{T}} = \mathbf{S_x}$, and $\mathbf{v}$ is a random vector of uncorrelated normally distributed values with zero mean and unit variance.

Small-scale structures are added to ECMWF temperature and humidity profiles ($\mathbf{t}_{\mathrm{E}}$ and $\mathbf{q}_{\mathrm{E}}$) following Equation (3) as

$$\mathbf{t} = \mathbf{t}_{\mathrm{E}} + \mathbf{K}_t \mathbf{v}, \tag{4}$$

$$\mathbf{q} = \mathbf{q}_{\mathrm{E}} + \mathbf{K}_q \mathbf{v}, \tag{5}$$

where $\mathbf{K}_t$ and $\mathbf{K}_q$ are the Cholesky decomposition of the covariance matrices describing the statistical properties of the additional terms. These covariance matrices can either be based on empirical data (such as radiosonde measurements) or be parametrized in different ways. If a first-order autoregressive model is applied for the random term, the following covariance matrix structure is obtained (Rodgers, 2000)

DOI: 10.1002/qj

$$S_{i,j} = \sigma^2 \exp\left(\frac{-|z_i - z_j|}{h}\right), \quad (6)$$

where $S_{i,j}$ is the covariance value corresponding to vector elements i and j, σ is the assumed standard deviation, z_i and z_j are altitudes for elements i and j , and h is the length-scale at which the inter-level correlation has exponentially decreased to $\exp(-1)$, here denoted as the correlation length.

The covariance model of Equation (6) is assumed throughout below, with a standard deviation of 0.5 K for temperature and 5% for humidity (in volume mixing ratio, VMR). The correlation length is set to 1 km at surface level and increases with altitude, to reach 3 km in the uppermost troposphere. From a literature search, no information relevant for the selection of the correlation length parameters was found, so these are chosen rather arbitrarily. We do not consider these as very important parameters, since they are used only to add small-scale structure to the humidity and temperature profiles from ECMWF. These small-scale structures will not be resolved by submillimetre passive down-looking measurements, and can be considered as 'geophysical noise' in the training data.

Humidity is expected to be close to saturation inside cloud layers, and humidity profiles are further modified to reflect this fact. The relative humidity (with respect to ice, RH_{i}) inside cloud ice layers is here assumed to have a mean value of 100% and a standard deviation of 10% (Ovarlez *et al*., 2002), with correlation lengths as for VMR humidity. A profile for saturated conditions ($\mathbf{r}(RH_i)$ with corresponding $\mathbf{q}_r$ (VMR)), extending over all altitudes, is created as

$$\mathbf{r} = \overline{\mathbf{r}} + \mathbf{K}_r \mathbf{v}, \quad (7)$$

where $\overline{\mathbf{r}}$ is the assumed mean state (100% RH_{i}) and $\mathbf{K}_r$ is the Cholesky decomposition of the covariance matrix for humidity variations inside cloud layers. The two humidity profiles are then weighted together to a final humidity profile as

$$\mathbf{q}_{\mathrm{f}} = (\mathbf{W}_q^{-1} + \mathbf{W}_r^{-1})^{-1}(\mathbf{W}_r^{-1}\mathbf{q} + \mathbf{W}_q^{-1}\mathbf{q}_r), \quad (8)$$

where $\mathbf{W}_r$ and $\mathbf{W}_q$ are diagonal weighting matrices. The diagonal elements i of $\mathbf{W}_r$ and $\mathbf{W}_q$ are

$$W_{r_{ii}} = \sigma_{r_i}^2 + \epsilon_1 \quad (9)$$

and

$$W_{q_{ii}} = 1 - \sigma_{r_i}^2 + \epsilon_2 \quad (10)$$

respectively, with

$$\sigma_{r_i} = 1 - \exp(-a w_i), \quad (11)$$

and ϵ_1 and ϵ_2 are small numbers ensuring the elements of the diagonal of $\mathbf{W}_r$ and $\mathbf{W}_q$ are greater than zero, a ($\mathrm{g}^{-1}\mathrm{m}^3$) is a scaling factor, w_i is the IWC ($\mathrm{g\ m}^{-3}$) value at the altitude corresponding to i, where the values at this stage are obtained from empirical relationships between radar backscatter, temperature, and IWC following Hogan *et al*. (2006). The scaling factor a was set to 10 $\mathrm{g}^{-1}\mathrm{m}^3$. In this way, with increasing amount of ice at a given altitude, the perturbed ECMWF humidity profile will be increasingly modified to be at saturation level.

As an example, if the IWC is above 1 gm^{-3} at a given level, almost 100% weight will be given to the saturation profile, and if the IWC is below 10^{-3} gm^{-3}, effectively 0% weight will be given to the saturation profile. Figure 1 shows practical examples of all profiles involved in the generation of a final humidity profile.

Down-looking submillimetre-wave observations may also be influenced by liquid clouds, hence these are also included in the scenarios. Liquid water content profiles are taken from the CloudNET level 2 meteorological products (linear scaled adiabatic method) and are averaged in the same way as the radar backscatter profiles. The distribution derived by Deirmendjian (1963) is used as liquid water PSD, while simulating radiative transfer through liquid clouds.

3.3. Ice cloud microphysical parameters

3.3.1. Particle size distribution

In the literature the PSD parameters are mainly parametrized as functions of temperature and IWC, or temperature alone (McFarquhar and Heymsfield, 1997; Ivanova *et al*., 2001; Heymsfield, 2003b). There is also evidence that the parameters are correlated with the distance from the cloud top (van Zadelhoff *et al*. 2004). Our aim is to use as few spurious correlations as possible. Here we only use correlations between the PSD parameters and temperature, but the scheme could easily be updated, as our knowledge of ice cloud increases. What is really important is that all possible states are covered, which in principle is easier to achieve if we assume no correlations between parameters. The PSD has been observed to follow a single or bimodal gamma size distribution in various *in situ* measurement campaigns (Ivanova *et al*., 2001; Heymsfield, 2003b). A bimodal gamma PSD can be written as

$$n(D) = \sum_{i=1}^{2} N_i D^{\mu_i} \exp(-\lambda_i D), \quad (12)$$

where $i = 1, 2$ here denotes the distribution for small and large particles respectively, D is the maximum dimension of the particles, μ_i is the width and λ_i is the slope of the distribution, and N_i is the intercept parameter determined by the IWC, w. N_i is given by

$$N_i = \frac{c_i w \lambda_i^{\beta_i + \mu_i + 1}}{\alpha_i \Gamma(\beta_i + \mu_i + 1)}, \quad (13)$$

DOI: 10.1002/qj

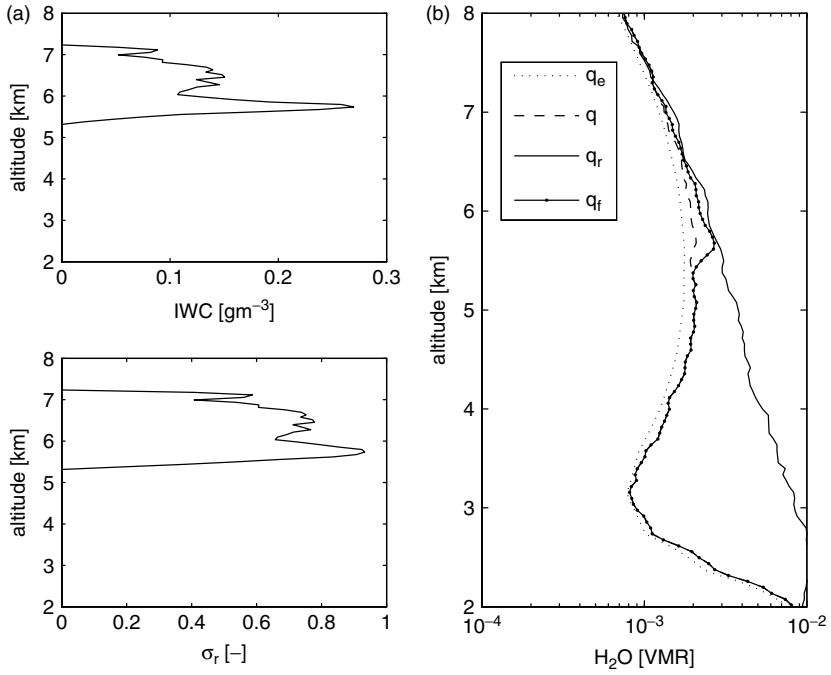

Figure 1. Practical example of the generation of humidity profiles. (a) shows the IWC profile, (b) the corresponding weight for the 'saturated' profile, and (c) all humidity profiles involved.

where c_i is the relative amount of IWC in the modes, Γ is the gamma function, α_i and β_i are related to the mass, m, of the particles by

$$m(D) = \alpha_i D^{\beta_i}. \tag{14}$$

Heymsfield (2003a) gives the values $\alpha_2 = 206$ gm$^{-\beta_2}$ and $\beta_2 = 2.25$ for midlatitude large ice particles. We assume that the small particles are solid ice spheres, and hence the density is $\rho = 917000$ g m^{-3}, $\alpha_1 = \rho\pi/6$, and $\beta_1 = 3$. Here the α_i and β_i parameters are treated as constants throughout. Furthermore, from Equations (12) and (13), it can be seen that the IWC, w, determines only a change of the magnitude of the PSD. The shape of the PSD can thus be described by 5 parameters (λ_1, λ_2, μ_1, μ_2, c_1, and $c_2 = 1 - c_1$). For the generation of cloud cases, a Gaussian variability of these parameters around their mean values was assumed; mean values and standard deviations are summarized in Table I. The standard deviations of the λ_2, μ_2, c_1, and c_2 parameters are not stated explicitly in cited articles, so the variability for these variables was estimated by inspection of figures in the references. Figure 2 displays a scatter plot of the λ and μ parameters of the large mode ($i = 2$), for values given in Table I. The figure can be directly compared to Figures 3(b) and (d) in Heymsfield (2003b).

The variables in Table I are either constant or depend only on temperature. Observations show that particles tend to be larger at the cloud base than at the cloud top. Note that the temperature dependency is such that the PSD is broadened for higher temperatures. This causes a higher fraction of larger particles towards the cloud base, because the temperature is higher at the cloud base. We have only found statistical information

Table I. Particle size distribution parameters.

Parameter	Value	Standard deviation	Information source
λ_1 (m^{-1})	154740	55415	Ivanova *et al.* (2001)
λ_2 (m^{-1})	$T > -18\,^\circ$C: 580 e$^{-0.114T}$ $T < -18\,^\circ$C: 2025 e$^{-0.042T}$	$0.25\lambda_2$	Heymsfield (2003b)
μ_1 (–)	3.24	1.41	Ivanova *et al.* (2001)
μ_2 (–)	$0.076\ (\lambda_2)^{0.80} - 2$	$0.02\ (\lambda_2)^{0.80}$	Heymsfield (2003b)
c_1 (–)	0.11	0.05	Ivanova *et al.* (2001)
c_2 (–)	$1 - c_1$	0.05	Ivanova *et al.* (2001)

See text for parameter definitions.

on the local variability, and the vertical correlation of variations of the size distribution variables is modelled as for temperature and humidity (using Equation (3), same correlation lengths, etc.). This approach should give more realistic results than either generating individual random values for each altitude (no correlation), or perturbing the values with random values common for all altitudes (complete correlation).

3.3.2. *Particle shape distribution*

The shape of individual ice particles has been shown to be highly variable and irregular (Korolev and Isaac, 2003; Heymsfield, 2003b). Furthermore, the shape distribution

DOI: 10.1002/qj

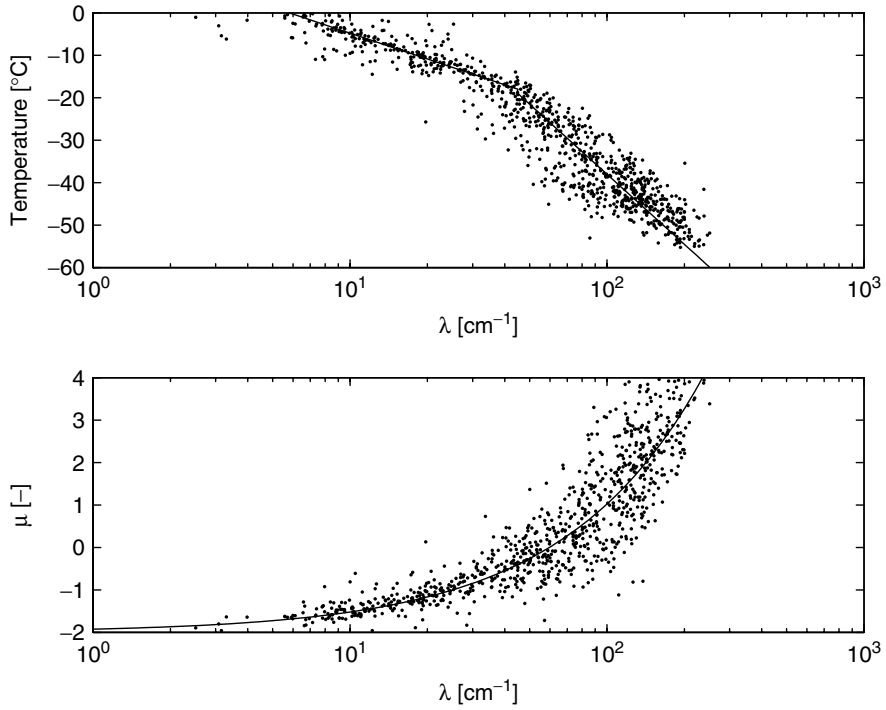

Figure 2. Scatter plots of the large mode λ_2 and μ_2 parameters used in the study. Solid lines represent mean values.

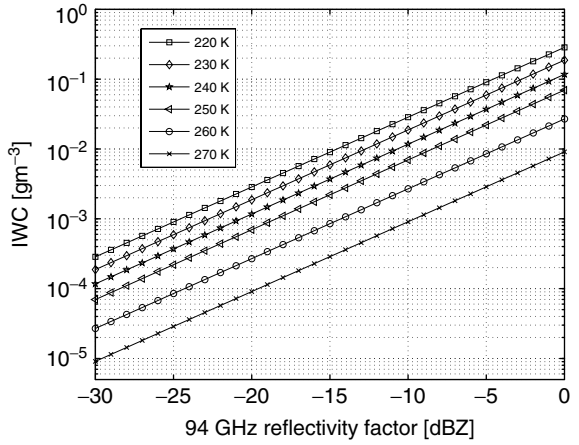

Figure 3. IWC–dBZ–temperature relationship in this study for a 94 GHz radar, for mean microphysical parameter values.

of ice particles is highly variable from cloud to cloud (Heymsfield and McFarquhar, 2002). On the other hand, the averaged aspect ratio (the ratio between horizontal and vertical dimension) of ice particle populations is generally well below 2, and the averaged aspect ratio for particle populations does not vary significantly with size for particles in the size range 60–1000 μm (Korolev and Isaac, 2003). It would be impractical to aim at representing all possible particle shapes, therefore simplifications must be made. An important consideration is that the calculation of single-scattering properties (SSP) is prohibitively expensive for most particle shapes. Only for a few simple shapes can SSP be easily calculated. We thus assume that the overall radiative properties can be modelled with a few particle shapes, with particle shape/size distribution as

$$n(D) = \sum_{j=1}^{n} s_j \sum_{i=1}^{2} N_i D^{\mu_i} \exp(-\lambda_i D), \qquad (15)$$

where j here denotes the particle shape, and s_j is the relative amount of IWC having that specific shape. In reality, an ice cloud consists of particles having many different shapes. If we assume that n is very large in Equation (15), the calculated averaged ensemble scattering properties of two similar clouds tend to be very similar. If n is small, then the ensemble scattering properties depend more on the shapes that have been included in the clouds. Since our knowledge of ensemble scattering properties is limited, and with respect to covering all possible ensemble scattering property scenarios, it is better to include a relatively few particle shapes in each scenario, than include very many particle shapes. A similar argument holds for representing the size distribution with a single size distribution for all shapes. This will give rise to a larger spread, compared to representing each assumed shaped with a specific size distribution. Section 3.3.3 provides more discussion on the particle shape assumptions. Particle shapes used here are spheres, ellipsoids, and cylinders, and each cloud profile contains a mixture of these three shapes. The aspect ratios of the ellipsoids and cylinders are here assumed to be in the range from 1 to 2.5. The aspect ratio is fixed for each particle shape and database case, and is selected with a uniform probability. The s_j of each particle shape is assumed to be normally distributed around 33% with a standard deviation of 10%. Vertical correlation is modelled as for humidity and temperature.

DOI: 10.1002/qj

3.3.3. *Single scattering properties*

A particle's SSP, for a given wavelength, depends on shape, size, refractive index, and orientation. Only relatively few particle shapes are included here (spheres, ellipsoids, and cylinders, Section 3.3.2). It is clear that this is a poor representation of real conditions, but this is of less importance here. The important question is whether realistic particle ensemble scattering properties are obtained. The phase function for a complex-shaped particle can be highly structured. However, we assume that for a particle ensemble, detailed structure of individual particles' phase functions are averaged out to a smooth phase function, as will be the case for the shapes considered here. The calculation of SSP can be achieved for the considered shapes by using the T-matrix code by Mischenko and Travis (1998). The SSP are calculated assuming solid ice particles, with the refractive index of pure ice.

The PSD (Section 3.3.1) is defined for the maximum dimension of the particles. Applying this size variable for the calculation of SSP for (e.g.) spheres would result in an overestimation of the scattering strength. The SSP are instead calculated for particles with mass equivalent size D_{s}, which is obtained by means of the maximum dimension–mass relationship of Equation (14). The equivalent mass sphere diameter for large ice particles is then

$$D_{\mathrm{s}} = \left(\frac{\alpha_2 6}{\rho\pi}\right)^{1/3} D^{\beta_2/3}. \tag{16}$$

The smaller ice particles have often been observed as quasi-spherical (Korolev and Isaac, 2003) and no size transformation is performed for the small particle mode.

Ice particles generally fall with a preferred orientation; flat crystals tend to orient with their maximum projected area orthogonal to the fall direction. The particles are generally randomly oriented azimuthally (Heymsfield, personal communication). An exception would be if strong local electric fields are present, which can orient the particles azimuthally, as observed by Caylor and Chandrasekar (1996). The calculation of SSP using the T-matrix code by Mischenko and Travis (1998) is flexible, since it can be performed for different particle orientations, e.g. totally randomly oriented particles, and azimuthally randomly oriented particles. Azimuthally randomly oriented particles will more likely give rise to polarization effects of radiance, and this effect has been observed in satellite data by Davis *et al.* (2005b).

3.4. Ice water content profiles

A combination of a radar backscatter profile and particle size and shape parameters has now been created. This combination of variables implies a specific IWC at each altitude. The IWC can be calculated by merging Equations (1), (13) and (15), to give

$$w = \frac{Z_{\mathrm{e}} 4\pi^4 |K_{\mathrm{w}}|^2}{\lambda^4} \frac{1}{\beta'}, \tag{17}$$

where

$$\beta' = \sum_{j=1}^{n} s_j \sum_{i=1}^{2} c_i \sum_{k=1}^{D_{\mathrm{m}}} \xi_b(D_{\mathrm{s},k}, \lambda_{\mathrm{r}}) \times D_{\mathrm{s},k}^2 \frac{\lambda_i^{\beta_i+\mu_i+1}}{\alpha_i \Gamma(\beta_i+\mu_i+1)} D_k^{\mu_i} \exp(-\lambda_i D_k) \Delta D. \tag{18}$$

The integral over the size spectrum from 0 to ∞ in Equation (1) has been replaced by a summation up to $D_{\mathrm{m}} = 0.05212\lambda_2(T)/100^{-0.81}$ m (Heymsfield, 2003b), where D_{m} is the largest particle size that has been observed for a given temperature from *in situ* measurements. By calculating IWC by Equation (17), each case in the database will be consistent with the measured radar signal. This approach should result in more realistic simulations, compared to the alternative approach of combining externally retrieved IWC with microphysical assumptions.

Figure 3 displays the relationships between dBZ and IWC arising from this work. The relationship has a clear temperature dependence. For lower temperatures, more IWC is needed to explain a measured dBZ value, owing to the fact that the number of larger particles decreases at lower temperatures. The methodology presented could accordingly also be used to retrieve IWC from the radar measurements. However, this is not the objective here, and in any case the cloud states in the database do not represent best IWC estimates, since microphysical parameters are generated in a stochastic way.

The method described results in highly structured IWC profiles. Figure 4(b) shows examples of IWC profiles thus obtained. Although the figure displays a time sequence of states, it can be seen that successive profiles can have a large degree of variation.

3.5. Generation of radiance

The second part of the database generation consists of simulating the radiance vector corresponding to the generated combination of atmospheric state and cloud microphysical state. The simulations were performed using version 1.1 of the Atmospheric Radiative Transfer Simulator (ARTS). This is a development of an earlier version (ARTS-1, Buehler *et al.*, 2005a), where two scattering modules, a discrete ordinate iterative method (Emde *et al.*, 2004) and a reverse Monte Carlo algorithm (Davis *et al.*, 2005a) have been implemented to solve the polarized radiative transfer equation in the presence of scattering. The polarization state is expressed by the Stokes formalism, the geoid and surface can have arbitrary shape, and atmospheric fields can have variations in three dimensions. The discrete ordinate iterative method has been used, since this module is more time efficient for 1D simulations. This scattering module can handle both types of particle orientation that are of interest here, i.e. completely randomly oriented particles and azimuthally randomly oriented particles.

DOI: 10.1002/qj

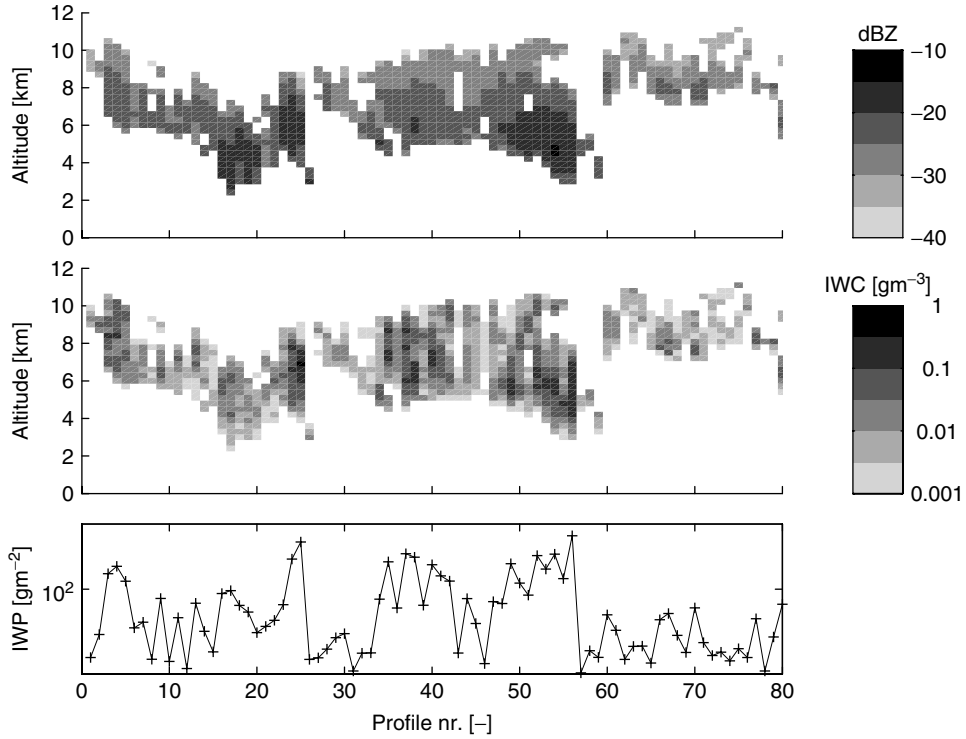

Figure 4. (a) averaged radar backscatter profiles. (b) IWC profiles that are generated from the radar backscatter profiles by the algorithm described. (c) IWP of the IWC profiles.

3.5.1. Example results

The Cloud Ice Water Sub-millimetre Imaging Radiometer (CIWSIR) is a submillimetre-wave satellite mission that has been proposed in the current ESA call for Earth Explorer Missions (Buehler, 2005). The scheme presented here was developed and used within the ESA-funded study 'Establishment of mission and instrument requirements to observe cirrus clouds at submillimetre wavelengths'. The training database can be used in the development/optimization phase of an instrument in order to estimate the retrieval performance for different channel selections (Jiménez *et al*., 2007).

CIWSIR is dedicated to measure IWP and the effective particle size of ice clouds. The instrument is suggested to be a conical scanner, with a footprint resolution of around 10 km, with a platform height of about 840 km, giving global coverage in about a day. Simulations of radiances have been performed here for the 12 suggested channels of CIWSIR which are: 183 ± 1.5, 3.5, 7 GHz, 243.2 ± 2.5 GHz, 325.15 ± 1.5, 3.5, 9.5 GHz, 448 ± 1.4, 3, 7.2 GHz, 664 ± 4 GHz, and 874 ± 6 GHz. In these simulations a single frequency representing each channel was used, and any spectral differences between the two side bands were ignored. The orientation of the particles was assumed to be azimuthally randomly oriented. Figure 5 shows examples of simulated radiances, expressed in the equivalent physical temperature of a black body (brightness temperature, T_b), for the 12 CIWSIR channels considered here, and for a variety of cloud and atmospheric states. It can be seen that the higher frequency channels have high response to high-altitude ice clouds, and the induced T_b depression can be up to 70 K for such cases.

4. Comparison with AMSU

Data from NOAA-15 AMSU-B water vapour channels 18–20 (183.3 ± 1, 3, 7 GHz) and AMSU-A channels 6–8 (54.40, 54.94 and 55.5 GHz), collected during 2003 and 2004 over the radar stations, are here compared to simulated radiances, in order to perform a first-order validation of the described method. However, such a comparison is not straightforward, mainly because the radars measure an approximate 2D cross-section, while the atmosphere covered by the AMSU footprint is a 3D volume. Accordingly, large differences can be expected in one-to-one comparisons, but the statistics for the two datasets should be required to be similar.

4.1. AMSU characteristics

AMSU-A and AMSU-B are cross-track scanning radiometers (Goodrum *et al*., 2000) which scan the atmosphere in 30 (90) steps, with viewing-angle steps of 3.3° (1.1°), within ±48.95°. AMSU-A and AMSU-B have together 20 channels, but only channels 6–8 (AMSU-A) and the three AMSU-B water vapour channels 18–20 are considered. Channels 6, 7 and 8 have 400, 400 and 330 MHz passbands respectively, whereas channels 18, 19 and 20 have 500, 1000 and 2000 MHz passbands respectively. The polarization response is such that at

DOI: 10.1002/qj

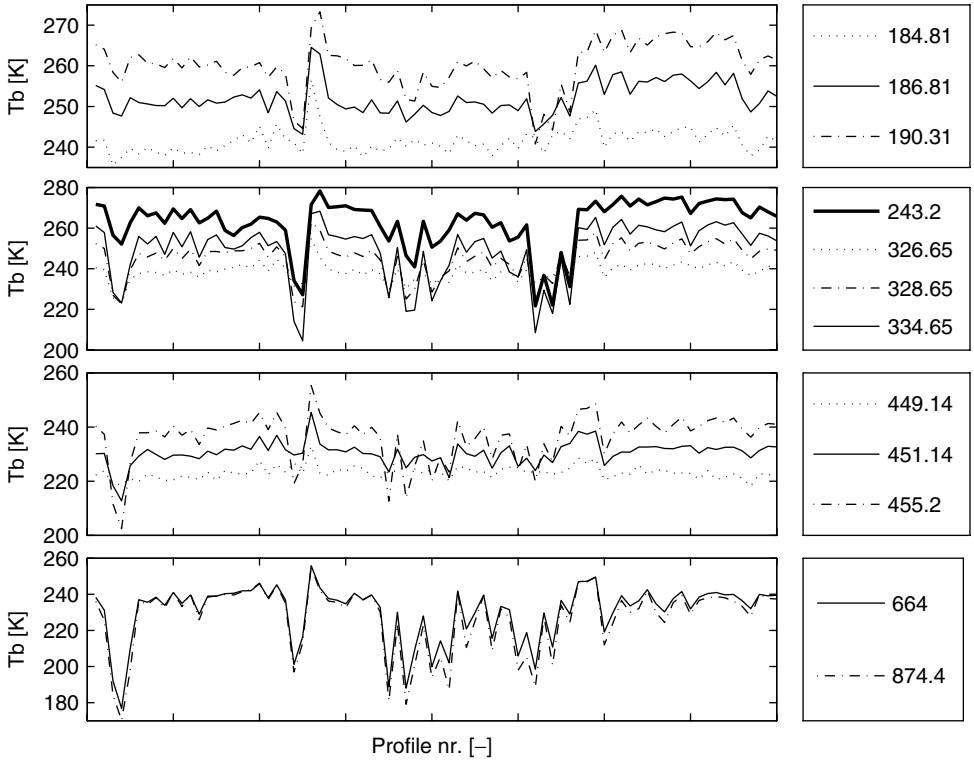

Figure 5. T_b simulations for the CIWSIR channels for a variety of cloud states. See Figure 4 for the underlying IWC profiles.

nadir the instrument is sensitive to only the vertical component of the radiation, and at other viewing angles to a combination of both vertical and horizontal polarization. More precisely:

$$T_{bm} = T_{bv} \sin^2(90 - \theta) + T_{bh} \cos^2(90 - \theta), \qquad (19)$$

where T_{bv} and T_{bh} are the vertical and horizontal component of the intensity, and θ is the nadir angle. The ground resolution of AMSU-A and AMSU-B at nadir is 48.1 km and 16.0 km respectively, and at the outer field of view 149.1 × 79.4 km and 51.6 × 26.9 km.

NOAA-15 passes over the radar stations approximately twice per day. Data with the centre of the footprint within 8 km of the radar stations were considered in the comparison; this resulted in approximately 1600 coincident measurements.

4.2. Simulation of AMSU radiance

The AMSU simulations were performed by taking into account the polarization response, and selecting three frequencies (the lowest, middle, and highest) for each passband. Furthermore, a second-degree polynomial was fitted over the bandwidth, and the mean of this fit over the passbands was reported as the simulated measurement.

The assumptions about particle shapes were as described in Section 3.3.2. Each cloud held a mixture of three particle shapes, and the orientation of the particles was either completely randomly oriented or azimuthally randomly oriented. The orientation of particles for a given shape was fixed; e.g. one specific cloud state consisted of spheres, azimuthally randomly oriented ellipsoids with aspect ratio 1.3, and randomly oriented cylinders with aspect ratio 1.4.

The surface emissivity was assumed to be log-normally distributed around 0.95, with a surface temperature equal to the lowermost temperature in the atmospheric profile. A 1D atmosphere was assumed, using climatological profiles for O_2, O_3, and N_2.

4.3. Comparison results

Different averaging lengths (Section 3.1) were considered, in an attempt to decrease the impact of the different observation geometries of AMSU and the radars. The radar data were averaged over ±0.5 km, ±8 km, ±16 km, ±32 km, and ±64 km, with respect to the time of the AMSU passages and the wind speed at 6 km. No large differences were found for the set of averaging lengths, largely because the statistics are dominated by conditions of clear sky and relatively thin clouds. The averaging length of ±32 km was then selected to cover an effective area roughly matching the size of the AMSU footprint. A selection just focusing on the influence of more dense ice clouds could have resulted in another averaging length.

AMSU-A channels 6–8 are basically not influenced by ice clouds, and are only considered in order to validate that the temperature and humidity profiles are treated properly. Sreerekha (2005) has shown that AMSU-B channels 18 and 19 also exhibit little influence of ice clouds at midlatitudes, and our simulations confirm this.

DOI: 10.1002/qj

The agreement between simulations and observations for channels 6–8 and 18 was very good, with only small biases and similar higher-order statistics (not shown). For the case of channel 19, the agreement was not satisfactory, with a ∼1.7 K bias, AMSU being warmer than simulations. However, channel 19 on NOAA-15 has been reported problematic (e.g. Buehler *et al*., 2005b).

By concluding that the atmospheric background states are treated properly, we turn our focus to AMSU-B channel 20, which is here the only channel where ice clouds significantly influence the measurements. Figure 6 shows scatter plots of AMSU-B channel 20 data and simulated measurements, where both liquid and ice clouds have been taken into account (full-sky simulations) and omitted (clear-sky simulations), for coincident radar measurements. In the figure, only cases are included where the database states have an IWP above 1 g m^{-2} (∼450 cases), to put emphasis on cloudy conditions. The same data are displayed in Figure 7 as cumulative T_b distributions.

The T_b values found in the clear-sky simulations are throughout >255 K, while about 10% of the AMSU data are below this level, including values down to 230 K. The lowest values can only be explained by scattering at higher altitudes, for the conditions considered here. Very dry atmospheric conditions together with low surface emissivity can also result in very low T_b. However, this occurs mainly over ice-covered regions, which not is the case here. The simulations including ice clouds also result in a value below 230 K. However, the lowest T_b values coincide in just a few cases between the datasets. The reason for this is that high IWP is localized over smaller areas, and since AMSU and the radars measure over different areas, it is likely that most dense clouds are only registered by one of the instruments. A one-to-one comparison is accordingly difficult (Figure 6), and it is more useful to investigate the statistical distribution (Figure 7).

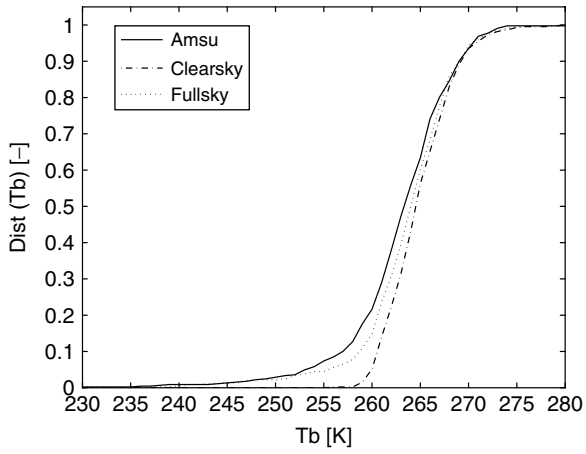

Figure 7. Cumulative distribution of measured AMSU-B channel 20 T_b, and simulated T_b based on co-located radar measurements, with ±32 km averaging.

Despite the fact that the 'full-sky' simulations manage to reproduce the level of lowest AMSU values, there is some underestimation of the impact of ice clouds, seen as a lower cumulative distribution between 250 and 260 K in Figure 7. The different geographical 'sampling' should be the main cause of the difference. AMSU is mainly sensitive to ice clouds which have a relatively high ice mass, which tend to be localized over smaller regions. It is more likely that AMSU rather than the radars would be influenced by such regions, since the AMSU footprint cover a larger volume. This should partly explain why our simulated T_b tends to be higher than AMSU. When the radar measurements' cross-sections pass through localized regions of high ice mass, the opposite occurs. In this case the difference between simulations and AMSU may also increase due to nonlinear relationships between

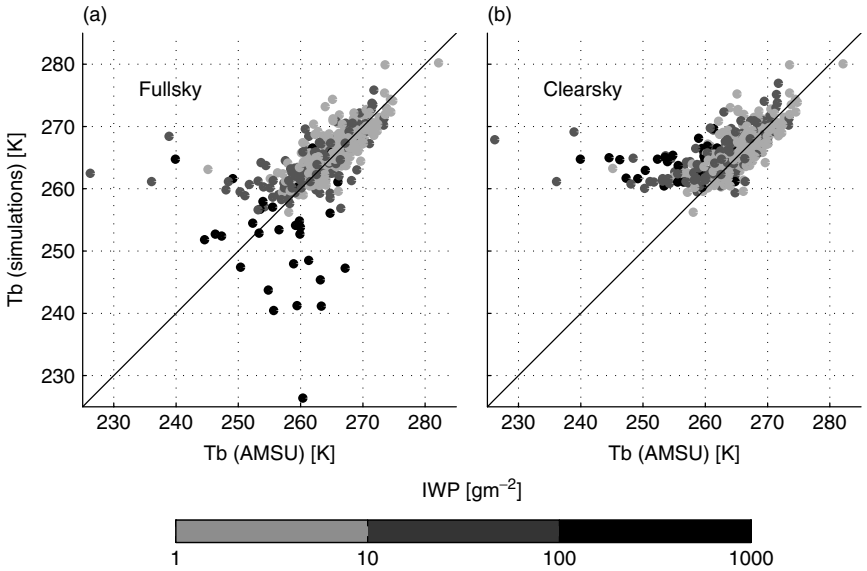

Figure 6. Scatter plots of measured AMSU-B channel 20 T_b, and simulated T_b based on co-located radar measurements, with ±32 km averaging, with (a) clouds included in the simulations, and (b) clouds omitted. The shading denotes IWP estimates from the radar measurements.

DOI: 10.1002/qj

ice cloud mass and T_b depression (Davis *et al*., 2006). For a given amount of ice mass, the highest T_b depression occurs if the ice mass is evenly distributed over the footprint. This corresponds to the situation in our 1D simulations. Although, this situation is less likely, it can explain why T_b simulations sometimes are considerably lower than AMSU measurements. It is also possible that there exists a systematic bias in applied microphysical variables. An underestimation of the fraction of largest particles for the cases corresponding to the 250–265 K range could contribute to the difference. An increased fraction of large particles would result in a higher T_b depression at the AMSU-B channel 20 frequencies, for a given IWC profile. This is because large particles are of higher importance at this wavelength. The issue is not pursued further here, but this discussion should stress the importance of multi-wavelength observations for more accurate IWP measurements.

5. Conclusions

A method to generate realistic ice cloud retrieval databases was developed. The database was generated by merging radar data and statistics from *in situ* measurements. The main advantage of the presented methodology is that simulated emission spectra are fully consistent with the radar observations, while at the same time the microphysical variables are given realistic variability. Only the generation of 1D atmospheric states is discussed, but the approach can be extended to 3D, by combining it with the work of Hogan and Kew (2005). The radiative transfer tool (ARTS) would handle this extension, but additional assumptions to model the horizontal correlation for variations of microphysical properties are required.

The method is presented using data from northern midlatitudes, mainly due to low availability of high-frequency radar data for other geographical regions. However, the recent release of CloudSat data (Stephens *et al*., 2002) changes this situation dramatically. Relevant radar data now exist with global coverage. Microphysical data for tropical simulations can be obtained from Heymsfield (2003b).

Simulated radiances were compared to AMSU measurements at the three considered radar stations (all in western Europe around 50 °N). It was shown that the inclusion of clouds is needed to describe the distribution of AMSU channel 20 data, while the impact of ice clouds on the other considered channels (6, 7, 8, 18 and 19) is small for midlatitude conditions. One-to-one comparisons with AMSU show large discrepancies, as non-identical air volumes are sampled, but the statistical distributions of AMSU channel 20 and simulated data show acceptable agreement, considering the limitations of the comparison.

The developed dataset has an unprecedented level of realistic detail with respect to the clouds' spatial, microphysical, and radiative properties. This should increase the confidence in retrieval simulations that are based on the dataset.

Acknowledgements

The authors acknowledge Ewan O'Connor for providing radar and ECMWF data from the Cloudnet archive, Viju Oommen John for providing co-located AMSU measurements, and Andy Heymsfield for advice on microphysical properties. This work was carried out inside an ESA funded project: 'Establishment of mission and instrument requirements to observe cirrus clouds at sub-millimetre wavelengths', ESTEC contract No. 19053/05/NL/AR. It is a contribution to COST Action 723 'Data exploitation and modelling for the upper troposphere and lower stratosphere'. COST: http://www.cost.esf.org

References

Buehler SA. 2005. Cloud Ice Water Submillimeter Imaging Radiometer (CIWSIR) – Mission Proposal. University of Bremen: Bremen. http://www/satpage/htdocs/projects/ciwsir/cirrus_expl_2005_08_12.pdf.

Buehler SA, Eriksson P, Kuhn T, von Engeln A, Verdes C. 2005a. ARTS, the Atmospheric Radiative Transfer Simulator. *J. Quant. Spectrosc. Radiat. Transfer* **91**: 65–93. DOI: 10.1016/j.jqsrt.2004.05.051.

Buehler SA, Kuvatov M, John VO. 2005b. Scan asymmetries in AMSU-B data. *Geophys. Res. Lett.* **32**: L24810. DOI: 10.1029/2005GL024747.

Caylor IJ, Chandrasekar V. 1996. Time-varying ice crystal orientation in thunderstorms observed with multi parameter radar. *IEEE Trans. Geosci. Remote Sensing* **34**: 847–858.

Cess RD. 1996. Cloud feedback in atmospheric general circulation models: An update. *J. Geophys. Res.* **101**: 12791–12794.

Davis CP, Emde C, Harwood RS. 2005a. A 3-D polarized reversed Monte Carlo radiative transfer model for millimeter and submillimeter passive remote sensing in cloudy atmospheres. *IEEE Trans. Geosci. Remote Sensing* **43**: 1096–1101.

Davis CP, Wu DL, Emde C, Jiang JH, Cofield RE, Harwood RS. 2005b. Cirrus induced polarization in 122 GHz Aura Microwave Limb Sounder radiances. *Geophys. Res. Lett.* **32**: L14806. DOI: 10.1029/2005GL022681.

Davis CP, Evans KF, Buehler SA, Wu DL, Pumphrey HC. 2006. 3-D polarised simulations of space-borne passive mm/sub-mm midlatitude cirrus observations: A case study. *Atmos. Chem. Phys. Discuss.* **6**: 12701–12728.

Deirmendjian D. 1963. 'Complete microwave scattering and extinction properties of polydispersed cloud and rain elements'. R-422-PR. Rand Corporation: Santa Monica. http://www.rand.org/pubs/reports/R422/.

Del Genio AD. 2002. GCM simulations of cirrus for climate studies. Chapter 15 of *Cirrus.* Oxford University Press: Oxford.

Emde C, Buehler SA, Davis CP, Eriksson P, Sreerekha TR, Teichmann C. 2004. A polarized discrete ordinate scattering model for simulations of limb and nadir long-wave measurements in 1-D/3-D spherical atmospheres. *J. Geophys. Res.* **109**(D24): D24207.

Eriksson P, Ekström M, Rydberg B, Murtagh DP. 2007. First Odin sub-mm retrievals in the tropical upper troposphere: Ice cloud properties. *Atmos. Chem. Phys.* **7**: 471–483.

Evans KF, Stephens GL, 1995. Microwave radiative transfer through clouds composed of realistically shaped ice crystals. Part II: Remote sensing of ice clouds. *J. Atmos. Sci.* **52**: 2058–2072.

Evans KF, Wiscombe WJ. 2004. An algorithm for generating stochastic cloud fields from radar profile statistics. *Atmos. Res.* **72**: 263–289.

Evans KF, Walter SJ, Heymsfield AJ, McFarquhar GM. 2002. Submillimeter-wave cloud ice radiometer: Simulations of retrieval algorithm performance. *J. Geophys. Res.* **107**: 2.1–2.21.

Evans KF, Wang JR, Racette PE, Heymsfield G. 2005. Ice cloud retrievals and analysis with the compact scanning submillimeter imaging radiometer and the cloud radar system during CRYSTAL FACE. *J. Appl. Meteorol.* **44**: 839–859.

Gasiewski AJ. 1992. Numerical sensitivity analysis of passive EHF and SMMW channels to tropospheric water vapor, clouds, and precipitation. *IEEE Trans. Geosci. Remote Sensing* **30**: 859–870.

Goodrum G, Kidwell KB, Winston W. 2000. 'NOAA KLM user's guide'. http://www2.ncdc.noaa.gov/docs/klm/.

Heymsfield AJ. 2003a. Properties of tropical and midlatitude ice cloud particle ensembles, Part I: Median mass diameters and terminal velocities. *J. Atmos. Sci.* **60**: 2573–2591.

Heymsfield AJ. 2003b. Properties of tropical and midlatitude ice cloud particle ensembles, Part II: Applications for mesoscale and climate models. *J. Atmos. Sci.* **60**: 2592–2611.

Heymsfield AJ, McFarquhar GM. 2002. Mid-latitude and tropical cirrus: Microphysical properties. Chapter 4 of *Cirrus.* Oxford University Press: Oxford, UK.

Hogan RJ, Kew SF. 2005. A 3D stochastic cloud model for investigating the radiative properties of inhomogeneous cirrus clouds. *Q. J. R. Meteorol. Soc.* **131**: 2585–2608.

Hogan RJ, Mittermaier MP, Illingworth AJ. 2006. The retrieval of ice water content from radar reflectivity factor and temperature and its use in evaluating a mesoscale model. *J. Appl. Meteorol.* **45**: 301–317.

IPCC. 2001. *Climate change 2001: The scientific basis*. Houghton JT, Ding Y, Griggs DJ, Noguer M, van der Linden PJ, Dai X, Maskell K, Johnson CA (eds). Cambridge University Press: Cambridge, UK.

Ivanova D, Mitchell DL, Arnott WP, Poellot M. 2001. A GCM parameterization for bimodal size spectra and ice mass removal rates in mid-latitude cirrus clouds. *Atmos. Res.* **59–60**: 89–113.

Jiménez C, Eriksson P, Murtagh DP. 2003. First inversions of observed sub-millimetre limb sounding radiances by neural networks. *J. Geophys. Res.* **108**(D24): 4791. DOI: 10.1029/2005GL022681.

Jiménez C, Buehler SA, Rydberg B, Eriksson P, Evans KF. 2007. Performance simulations for a sub-millimetre wave ice cloud satellite instrument. *Q. J. R. Meteorol. Soc.* **133**: 129–149.

John VO, Soden BJ. 2006. Does convectively-detrained cloud ice enhance water vapor feedback? *Geophys. Res. Lett.* **33**: L20701. DOI:10.1029/2006GL027260.

Korolev A, Isaac G. 2003. Roundness and aspect ratio of particles in ice clouds. *J. Atmos. Sci.* **60**: 1795–1808.

Li JL, Waliser DE, Jiang JH, Wu DL, Read W, Waters JW, Tompkins AM, Donner LJ, Chern JD, Tao WK, Atlas R, Gu Y, Liou KN, DelGenio A, Khairoutdinov M, Gettelman A. 2005. Comparisons of EOS MLS cloud ice measurements with ECMWF analyses and GCM simulations: Initial results. *Geophys. Res. Lett.* **32**: L18710. DOI: 10.1029/2005GL023788.

McFarquhar GM, Heymsfield AJ. 1997. Parameterization of tropical cirrus ice crystal size distribution and implications for radiative transfer: results from CEPEX. *J. Atmos. Sci.* **54**: 2187–2200.

Mishchenko MI, Travis LD. 1998. Capabilities and limitations of a current FORTRAN implementation of the T-matrix method for randomly oriented rotationally symmetric scatterers. *J. Quant. Spectrosc. Radiat. Transfer* **60**: 309–324.

Ovarlez J, Gayet JF, Gierens K, Ström J, Ovarlez H, Auriol F, Busen R, Schumann U. 2002. Water vapour measurements inside cirrus clouds in Northern and Southern Hemisphere during INCA. *Geophys. Res. Lett.* **29**(16): 1813. DOI: 10.1029/2001GL014440.

Rodgers CD. 2000. *Inverse methods for atmospheric sounding: Theory and practice*. World Scientific Publishing: Singapore.

Sreerekha TR. 2005. 'Effect of ice clouds on microwave radiances. Impact of clouds on microwave remote sensing'. PhD thesis, University of Bremen. Logos Verlag: Berlin.

Stephens GL, Vane DG, Boain R, Mace G, Sassen K, Wang Z, Illingworth A, O'Connor E, Rossow W, Durden SL, Miller S, Austin R, Benedetti A, Mitrescu C. 2002. The CloudSat mission and the A-train: A new dimension of space-based observations of clouds and precipitation. *Bull. Am. Meteorol. Soc.* **83**(12): 1771–1790.

van Zadelhoff GJ, Donovan DP, Klein Baltink H, Boers R. 2004. Comparing ice cloud microphysical properties using CloudNET and Atmospheric Radiation Measurement program data. *J. Geophys. Res.* **109**: D24214, DOI:10.1029/2004JD004967.